Available online at www.sciencedirect.com

ScienceDirect

Procedia Structural Integrity 28 (2020) 1536–1550

Structural Integrity Procedia

www.elsevier.com/locate/procedia

1st Virtual European Conference on Fracture

Numerical calibration of the direct current potential drop (DCPD) method in fracture mechanics fatigue tests

G. Meneghetti[a,*], L. Vecchiato[a], A. Campagnolo[a], P. Rech[a], M. Cova[b]

[a]*Department of Industrial Engineeering, University of Padova, Via Venezia 1, Padova, 35131, Italy*
[b]*SACMI Imola S.C., Ceramic Engineering Department, Via Selice Provinciale 17/A, Imola, 40026, Italy*

Abstract

Fatigue strength and fracture mechanics concepts are linked together by the so-called cyclic R-curve, i.e. the crack size dependence of the fatigue crack propagation threshold. The cyclic R-curve requires to identify experimentally the extension of a propagating crack in the mechanically short crack regime. One of the most used techniques adopted in experimental tests is the direct current potential drop (DCPD) method, according to which the electrical resistance of the tested specimen increases due to crack propagation and the resulting electric potential change is used to derive the crack length thanks to proper calibration curves. In this work, the DCPD technique was applied in fracture mechanics fatigue tests of carbon steel bars weakened by a single-edge, semi-elliptical pre-crack. First, it was assumed that the semi-elliptical pre-crack propagates under fatigue axial loading in such a way to keep an iso-stress intensity factor (SIF) K_I crack front. Accordingly, the corresponding crack pattern was derived by means of 3D structural FE analyses using the Peak Stress Method (PSM). Afterwards, the DCPD calibration curves were derived through 3D electrical FE analyses. The effects of the locations of the current and of the potential probes were investigated. Finally, a three-probe dual channel DCPD technique was applied to compensate any temperature variation of the tested specimen.

Peer-review under responsibility of the European Structural Integrity Society (ESIS) ExCo

Keywords: fatigue; direct current potential drop; finite element method; calibration curve; in-situ crack growth monitor

* Corresponding author. Tel.: +39-049-827-6751
E-mail address: giovanni.meneghetti@unipd.it

2452-3216 © 2020 The Authors. Published by Elsevier B.V.

Peer-review under responsibility of the European Structural Integrity Society (ESIS) ExCo
10.1016/j.prostr.2020.10.126

Nomenclature

a	crack depth
a/D	normalized crack depth
$2c$	major axis of the elliptical crack
c/a	crack aspect ratio
D	specimen net-section diameter
F	axial load
I	electrical current
K_I	stress intensity factor of a crack under mode I loading
$\Delta\nu_{PD}$	potential drop geometrical factor of the active channel
θ_I	angular position of the current probes
θ_{PD}	angular position of the active channel potential probes
θ_T	angular position of the potential probes for temperature compensation
ρ	electrical resistivity
S	curvilinear coordinate along the semi-elliptical crack tip profile
ΔV_{PD}	potential drop of the active channel
ΔV_T	potential drop of the reference channel for temperature compensation
Y_I	distance of the current probe from crack plane
Y_{PD}	distance of the active channel potential probe from crack plane
Y_T	distance of the reference channel potential probe from crack plane

1. Introduction

Fatigue crack propagation threshold is a parameter that has a fundamental role in fatigue life assessment of cracked structural components, which makes use of a damage-tolerant approach (Zerbst et al. 2016). Its value depends on many parameters including the crack size itself (Frost et al. 1971). The latter dependency is quantitatively described by the so-called cyclic R-curve, whose definition was firstly given by Tanaka and Akiniwa (1988). The experimental determination of the cyclic R-curve requires that the size of the fatigue crack, defined in the mechanically short crack regime, is known. Moreover, this kind of experimental tests requires very high accuracy in the determination of the near-threshold crack growth rate, *da/dN*, whose value can be assumed equal to 10^{-10} m/cycle which is the one fixed for long cracks by the ASTM E647-15 standard. Therefore, to save time to perform measurements, a crack growth monitor method having high sensitivity is required. Many experimental techniques are available to estimate the size of a propagating crack and one of these is the direct current potential drop method (DCPD), where the electrical resistance of the tested specimen increases due to crack growth; therefore, if the specimen is subjected to a constant electrical current flow, the increase of the electrical resistance translates in an increase of the potential drop. The crack depth, *a*, can be estimated by entering a proper calibration curve with the experimentally measured potential drop. Calibration curves can be derived either experimentally, analytically, or numerically. However, as highlighted by Campagnolo et al. (2018), the numerical calibration is preferable, since it is easier and less time-consuming and it allows to investigate the effects of both the crack shape and of the location of the potential and current probes on the calibration curves.

In the past, several authors have investigated different solutions to enhance the DCPD sensitivity and, therefore, to reduce the minimum detectable crack size increment during fatigue tests. Among these, Ritchie and co-authors (1971, 1979, 1979) analysed the effect of both current and potential probes locations on DCPD sensitivity dealing with flat specimens (CT, SEN). They concluded that the highest sensitivity can be obtained not only by injecting the current but also by measuring the potential drop as close as possible to the crack or notch tip. However, they also advised against this experimental configuration due to its strong sensitivity to positioning errors. Later on, also Saka e al. (1996) observed that current and potential probes localized at the crack tip can significantly enhance the DCPD sensitivity.

In this work, the application of DCPD to axial fatigue tests carbon steel round bars, weakened by a single-edge semi-elliptical pre-crack was investigated. In particular, the ultimate goal being the experimental derivation of the cyclic R-curve for the same specimen geometry, a numerical full-factorial design was performed to locate the potential and current probes in order to enhance the DCPD sensitivity. Indeed, the higher the DCPD sensitivity is, the smaller the detectable crack size increment and, therefore, the shorter the time to estimate a certain value of near-threshold crack growth rate, *da/dN*. Concerning the effect of the crack shape on the calibration curves, it was assumed that the semi-elliptical pre-crack propagates under axial fatigue loading by increasing its depth, *a*, and by changing its aspect ratio, *c/a*, in order to keep an iso-stress intensity factor (SIF) K_I crack front. Accordingly, the iso-K_I aspect ratio *c/a* was derived as a function of the crack depth *a* by means of 3D structural FE analyses using the Peak Stress Method (PSM), which is an engineering FE-oriented method to rapidly estimate the SIFs by using the singular linear elastic peak stresses calculated from coarse FE analyses (Meneghetti and Lazzarin, 2007). Once the iso-K_I crack shape was found versus the crack size, the calibration curves were obtained from 3D electrical FE analyses, where the DCPD sensitivity to the location of both the current and potential probes were investigated. Finally, the location of a third potential probe was analysed to define the reference channel of a three-probe dual channel DCPD configuration for compensating any temperature variation of the tested specimen.

2. DCPD calibration curves

The DCPD calibration curves report the potential drop, ΔV_{PD}, as a function of the crack depth, *a*. From a general point of view, there are two ways to enhance the sensitivity of a DCPD measurement:

- the first one is based on the measurement of smaller potential drop changes and, to do this, an experimental device with a higher resolution is required, while keeping fixed the DCPD experimental setup, i.e. the location of both the current and potential probes;
- on the other hand, the second one is based on a modification of the calibration curve, in order to detect smaller crack increments for the same value of the potential drop change. To do this, the DCPD experimental setup, should be optimised while keeping the same experimental device.

The present paper is focused on the second approach to increase the sensitivity of a DCPD measurement. To do this, first Ohm's law allows to clarify which parameters should be changed to enhance the sensitivity of the DCPD calibration curves :

$$\Delta V_{PD} = \rho I \Delta v_{PD} \tag{1}$$

Large values of the potential drop signal ΔV_{PD} are preferable because they are more easily measurable.

Furthermore, as proposed by Ritchie and Aronson (1979) and similarly to what was done by Van Minnebruggen et al. (2017), it is possible to estimate the DCPD sensitivity by evaluating the derivative of the potential drop ΔV_{PD} with respect to the crack size *a*, i.e. by evaluating the slope of the DCPD calibration curve:

$$\frac{d\Delta V_{PD}}{da} = \rho I \frac{d\Delta v_{PD}}{da} \tag{2}$$

Similarly to the potential drop ΔV_{PD}, large values of its derivative are more desirable to discriminate between small differences in crack length. Therefore, equations (1) and (2) suggest the directions to increase the sensitivity to crack growth of the experimental set-up:

- Electrical resistivity, ρ. This is a material property. Commonly the DCPD method is applied in fatigue testing of metal components, i.e. conductive materials. In such case, the values of the resistivity at room temperature are on the order of 10^{-5} Ω·mm. Equations (1) and (2) show that higher signals and sensitivity can be achieved with higher resistivity. For a given material, resistivity depends on variables like microstructure, plasticity and above all temperature. Concerning temperature variations, it is common practice in DCPD applications to compensate their effect by normalizing the potential drop signal ΔV_{PD}

with a reference potential drop signal ΔV_T measured on the same specimen (see next section 2.3). In this way, the calibration curve is independent of temperature changes.

- Electrical current, I. A higher electrical current leads not only to a higher potential drop signal ΔV_{PD}, but also to a higher sensitivity. Its value has to be chosen as high as possible to benefit the advantages described above but it has to be limited to avoid excessive overheating of the component due to Joule effect. Concerning this aspect, attention has to be paid to the electrical resistivity occurring in the contact area between the current probes and the specimen surface. Moreover, although the current value should be maintained as constant as possible without ripple and noise, the calibration curves can be made independent of the magnitude of the injected current by simply normalizing the potential drop signal ΔV_{PD} with a reference potential drop signal ΔV_T measured on the same specimen as discussed previously for the electrical resistivity.In standard in-field applications values of the applied current are commonly within 0.5 A and 50 A but they can be even higher (for example Van Minnebruggen et al. (2017) imposed a value of 150 A) depending on the employed experimental device and on the experimental setup.
- Potential drop geometrical factor, $\Delta \nu_{PD}$. This is a geometrical parameter including all the information about the shape of current density vector field; Therefore, it depends on the specimen geometry, the crack size and shape, the location of the current and potential probes. However, when considering a given specimen geometry, the propagating crack shape turns out to be dependent on both the specimen geometry and on the applied fatigue loading; this means that crack shape is not an input parameter, which can be changed or optimized, but, on the other hand, it can be estimated assuming a propagation criterion. Therefore, the location of the current and of the potential probes are the sole parameters that can be optimised so as to increase sensitivity of the DCPD setup.

2.1. Specimen geometry and iso-K_I crack shape

The considered specimen geometry is reported in Fig. 1 along with details of the single-edge semi-elliptical pre-crack. The material is a medium carbon steel, i.e. AISI 1045, with elastic modulus, Poisson's ratio and electrical resistivity (the latter evaluated at a reference temperature of 20°C) equal to 206000 MPa, 0.3 and $20{\cdot}10^{-5}$ Ω·mm, respectively.

It was assumed that the semi-elliptical pre-crack propagates under axial fatigue loading by increasing its depth, *a*, and by varying its aspect ratio, *c/a*, in order to keep an iso-stress intensity factor (SIF) K_I crack front. To evaluate the aspect ratio *c/a* corresponding to an iso-K_I crack front, 3D structural linear elastic FE analyses (Fig. 2) were carried out for different crack depths *a*. In particular, the normalized crack depth *a/D* was varied between 0.1 and 0.5, while the aspect ratio *c/a* was roughly included in the range from 1.0 to 2.5. Table 1 reports a summary of all structural FE analyses performed.

The K_I values along the crack tip were computed by taking advantage of the Peak Stress Method (Meneghetti and Lazzarin, 2007), which is an engineering FE-oriented method to rapidly estimate the SIFs on the basis of the singular, linear elastic, peak stresses calculated from coarse FE analyses. The mode I SIF was estimated according to PSM by applying the following expression (Meneghetti and Lazzarin, 2007):

$$K_1 \cong K^*_{FE} \cdot \sigma_{I,peak} \cdot d^{0.5} \tag{3}$$

where *d* represents the so-called "global element size", i.e. the average size of the FE elements adopted to generate a free mesh pattern; K^*_{FE} is a non-dimensional parameter, previously calibrated to take into account of: (i) element type and formulation, (ii) mesh pattern of finite elements and (iii) procedure to extrapolate stresses at FE nodes; while $\sigma_{I,peak}$ is the singular, linear elastic, opening peak stress component evaluated at the crack tip by a FE analysis according to the PSM (Meneghetti et al., 2018). All numerical models were analysed by using 3D, 10-node, tetrahedral, structural solid elements (SOLID187 of Ansys element library). The global element size was assumed equal to 1.5 mm, while close to the crack tip an element size of about 0.2 mm was obtained by applying a gradual mesh refinement. Such a refined FE mesh pattern was adopted to obtain a large number of K_I values and, therefore, to calculated accurately the K_I distributions along the crack tip. It should be noted that significantly coarser FE meshes could have been adopted according to PSM. As an example, to estimate the K_I distribution along the tip of the crack having minimum depth, i.e. a = 2.36 mm, the PSM would have required a mesh density ratio $(a/\mathrm{d})_{\min} = 3$ (valid for a crack analysed with 10-node tetra elements, as reported by Campagnolo et al., 2019), which corresponds to an element size at the crack tip of d = 2.36/3 ≈ 0.78 mm.

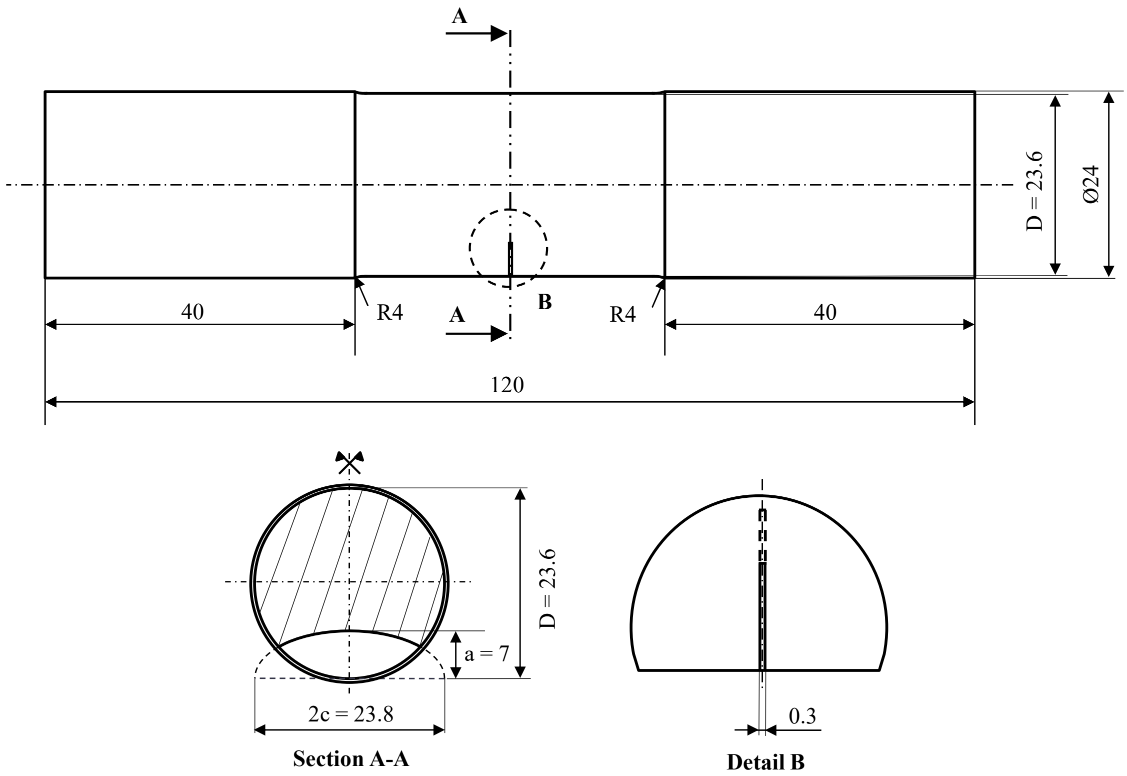

Fig. 1. Geometry of single-edge semi-elliptical pre-cracked specimen (dimensions are in millimetres)

Taking advantage of the XY and XZ symmetry planes only one-quarter of the specimen was modelled. Two different boundary conditions were simulated at the gripped sections. In the first case, the specimen gripped section was left free to translate and rotate so that machine grips were not simulated. Instead, in the second case, machine grips were simulated and all nodes belonging to the outer surface of the specimen gripped section were constrained to have fixed displacements in X and Z directions and the free displacement in the Y direction.

Table 1. Summary of the structural FE analyses carried out to derive the iso-K_I crack propagation pattern

a/D [-]	D [mm]	*c/a* [-]	Boundary conditions
0.1	23.6	1.0, 1.1, …, 1.5	Free, Simply supported
0.2		1.0, 1.1, …, 2.0	
0.3		1.5, 1.6, …, 2.5	
0.4		1.5, 1.6, …, 2.5	
0.5		1.5, 1.6, …, 2.5	

To simulate the axial loading, a uniformly distributed pressure was applied at the specimen's end, in order to generate a nominal stress of 1 MPa referred to the uncracked section having diameter of 23.6 mm (Fig. 1).

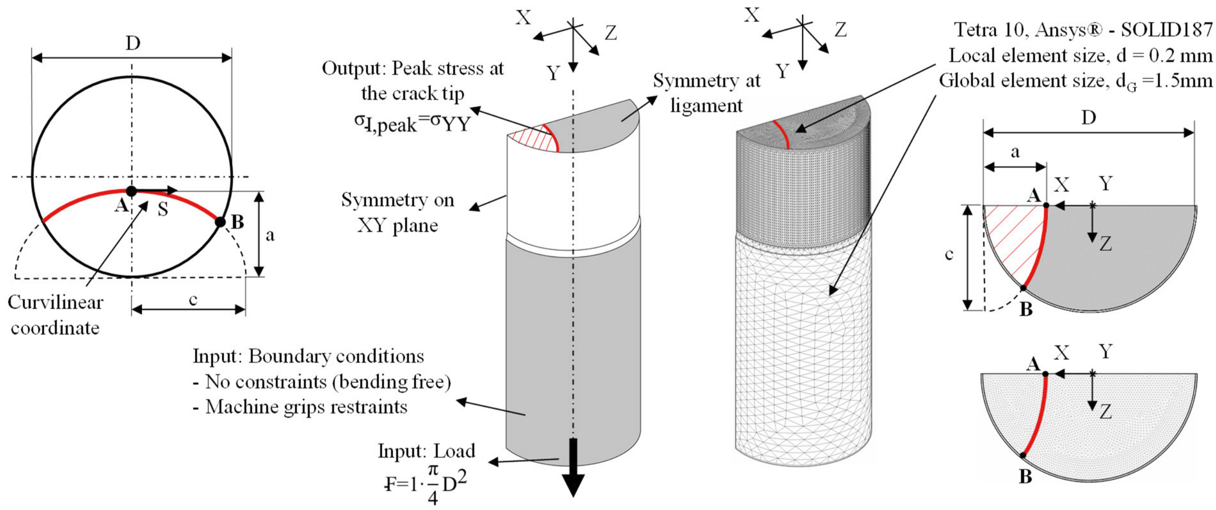

Fig. 2. 3D structural FE analyses to calculate the mode I SIF along the crack tip using the PSM.

The results obtained by the 3D structural FE analyses are shown in Fig. 3, where SIF values are reported as a function of the normalized curvilinear coordinate (S in Fig. 2 or in Fig. 3) for different values of the normalized crack depth *a/D*, aspect ratio *c/a* and boundary conditions ('Free' on Fig. 3a. and 'Simply Supported' on Fig. 3b). Figure 3 shows that the 'Simply supported' condition leads to even more reduced SIF values as compared to those relevant to 'Free' condition, as the crack depth *a/D* increase, while SIF values are almost the same for both considered boundary conditions when small crack depth (*a/D* = 0.1) are analysed.

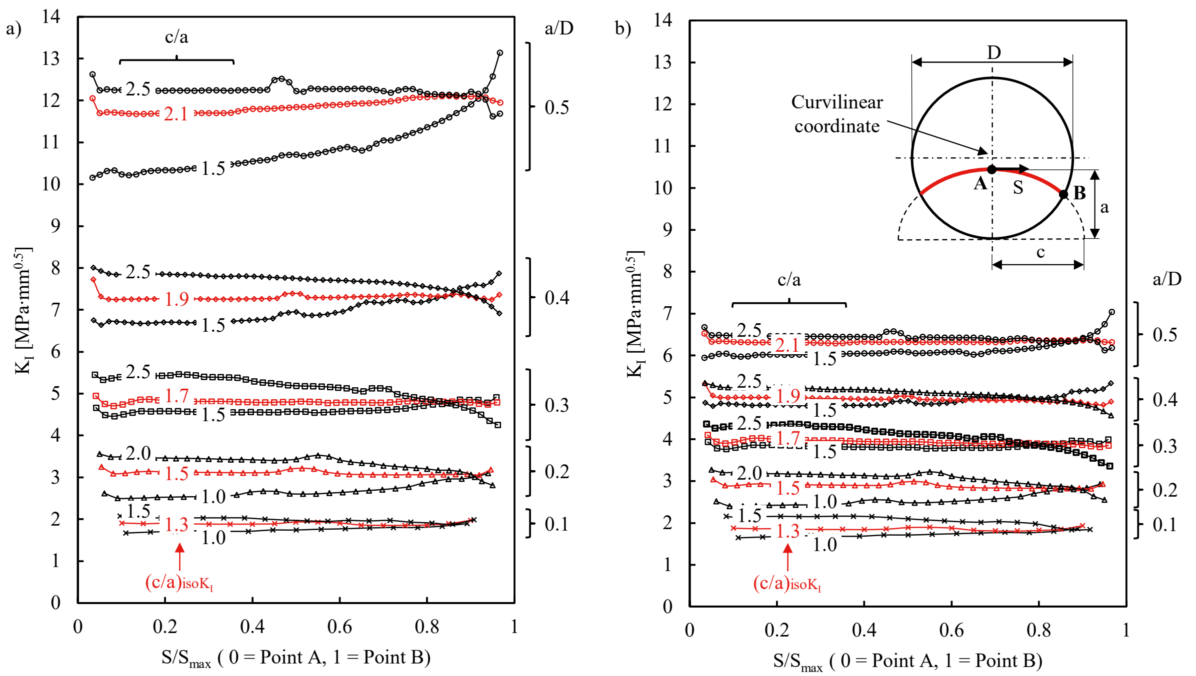

Fig. 3. K_I distributions derived by the PSM as a function of the normalized curvilinear coordinate, the aspect ratio *c/a* and the crack depth *a/D*. The K_I profiles are reported according to a) 'Free' boundary conditions; b) 'Simply supported' boundary conditions.

Moreover, for a given crack depth under both analysed boundary conditions, the SIFs profiles could assume higher values at the centre of the specimen (point A or S/Smax = 0) or at the surface of the specimen (point B or S/Smax = 1) depending on the aspect ratio *c/a*. More in detail, for low values of *c/a*, i.e. for very curved-fronted crack, the SIF maximum value was located on the external cylindrical surface of the specimen (point B), while for high values of *c/a* the SIF maximum value was located on the symmetry plane, at the point A. By analysing this trend, it was possible to identify intermediate values of aspect ratio *c/a* that generated crack shapes such as to have a roughly constant SIF profile, therefore fulfilling the iso-K_I criterion.

By analysing the K_I distributions derived by the PSM as a function of the normalized curvilinear coordinate reported in Fig. 3, the value of *c/a* corresponding to an iso-K_I distribution was correlated to each considered crack depth *a*. This relationship is reported in Fig. 4. The aspect ratio *c/a* which guarantees an iso-K_I crack profile was almost independent of the constraint condition applied to the specimens, i.e. 'Free' or 'Simply supported'. Moreover, a linear interpolation of the results seemed to be appropriate to describe the dependence of *c/a* on the normalized crack depth *a/D*, when an iso-K_I crack profile was assumed.

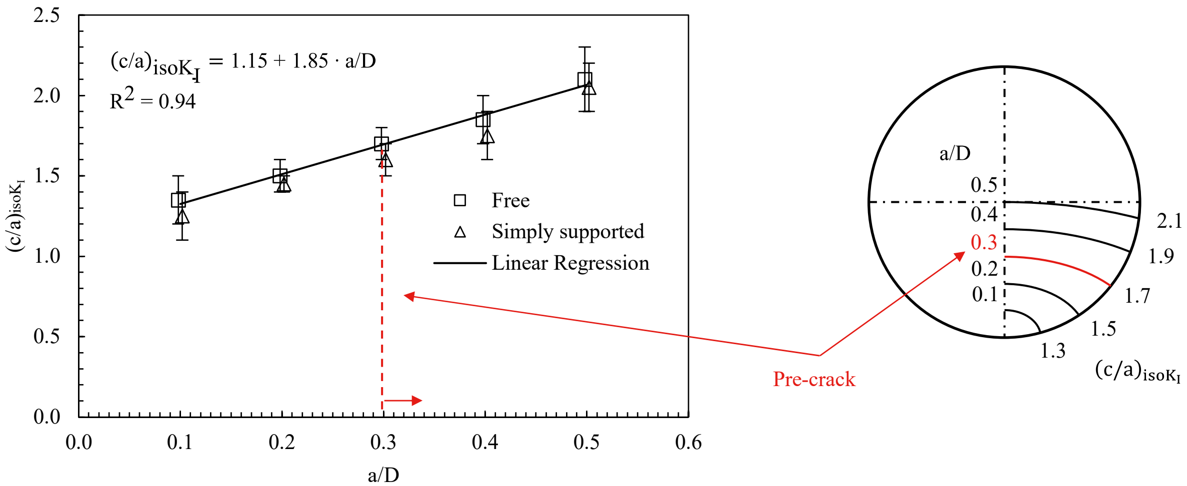

Fig. 4. Fatigue crack path according to iso-K_I criterion applied to the cylindrical specimen of Fig. 1.

2.2. Locations of current and potential probes

As previously discussed, the DCPD calibration curves depend on three main parameters, i.e. the electrical resistivity, the electrical current and the geometrical factor. It has been previously observed that the latter depends only on the locations of both current and potential probes, for a given specimen geometry and crack shape.

In the present paper, previous investigations performed in the literature dealing with flat specimens (Ritchie and co-authors, 1971, 1979, 1979) were extended to the cylindrical specimen shown in Fig. 1. To analyse the effects of the current and potential probe locations, the calibration curves were derived by means of 3D electrical FE analyses. All numerical analyses were performed using 3D, 10-node tetrahedral electric solid elements (SOLID232 of the Ansys element library). A global element size of 1.5 mm was adopted while an element size of about 0.7 mm was employed in the regions nearby the surface from which numerical results were extracted. Moreover, a mesh refinement leading to a local element size of about 0.3 mm was applied close to the crack plane. The current probe location was defined by the angular coordinate, θ_I, originating at the centre of the crack, and the axial coordinate, Y_I, i.e. the distance from the crack plane. Similarly, the potential probe location was defined by the angular coordinate θ_{PD} and axial distance Y_{PD}. Both current and potential probes were assumed to be symmetrically positioned with respect to the crack plane.

In order to investigate the effect of the current probe position on DCPD sensitivity in cylindrical specimens, four different current injection positions were considered.

Firstly, a remote current input was modelled (Fig. 5). In this case, the current probes were located far from crack surface ($Y_I = \infty$) to generate a uniform distribution of the current density upstream and downstream of it. The second configuration was dedicated to analyse the effect of a local current input, the probes being located at the XY symmetry plane ($\theta_I = 0°$) and at an axial distance from the crack plane $Y_I = 11.5$ mm (Fig. 6).

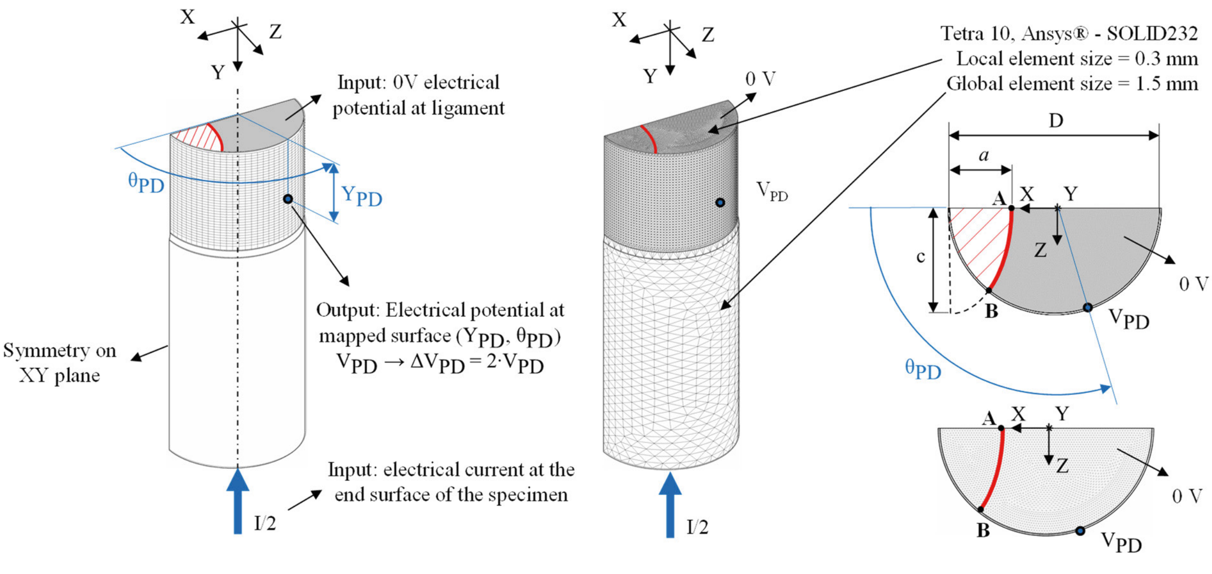

Fig. 5. 3D electrical FE analyses for calibrating the potential drop method: remote current input ($Y_I = \infty$).

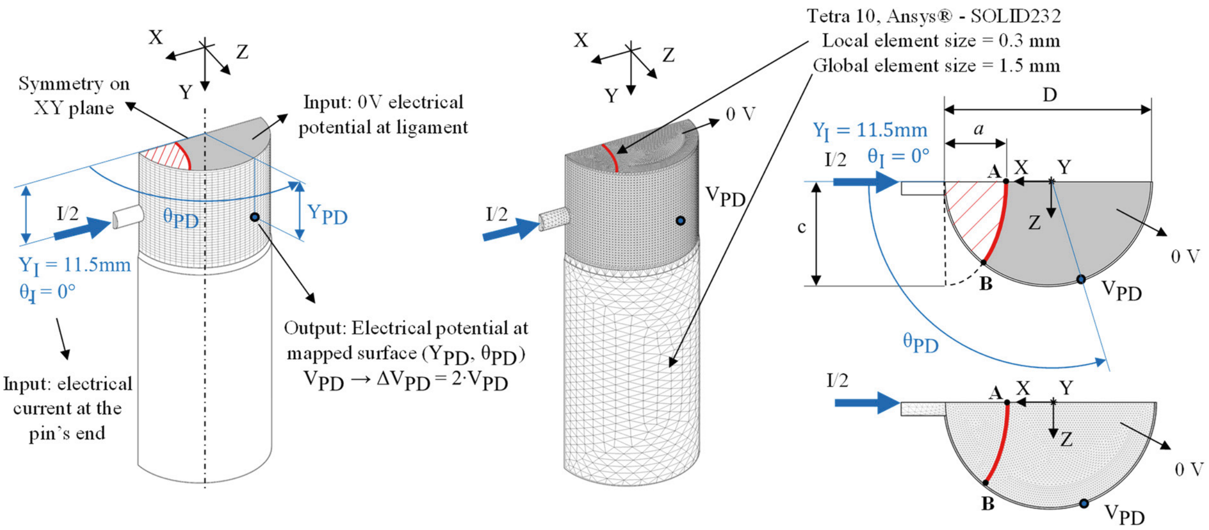

Fig. 6. 3D electrical FE analyses for calibrating the potential drop method: local current input ($Y_I = 11.5$ mm, $\theta_I = 0°$).

Finally, the last two configurations were designed to understand the effects of the axial distance (third configuration with $Y_I = 4$ mm and $\theta_I = 0°$, Fig. 7) or angular position (fourth configuration with $Y_I = 11.5$ mm and $\theta_I = 50°$, Fig. 8) of the current probes. Noteworthily, the configurations providing a local current input (second, third and fourth) were simulated by assuming that the current was injected through a cylindrical pin with a diameter of 3 mm, made of the same material of the specimen and without contact electrical resistance . In all cases, a constant direct current, I, of 50 A was injected in the specimen.

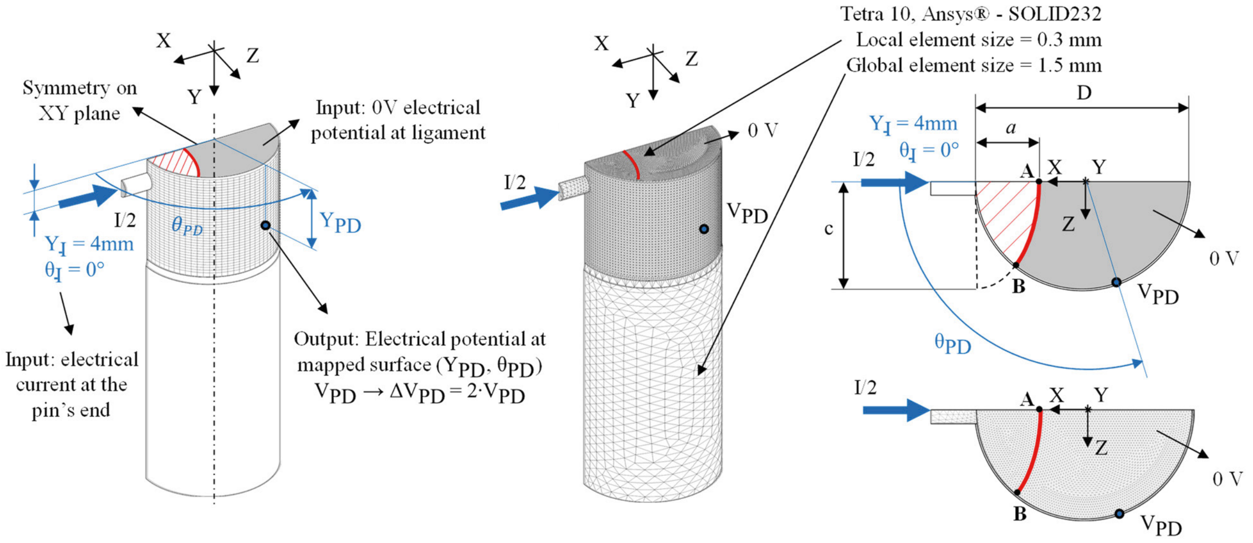

Fig. 7. 3D electrical FE analyses for calibrating the potential drop method: local current input ($Y_I = 4$ mm, $\theta_I = 0°$).

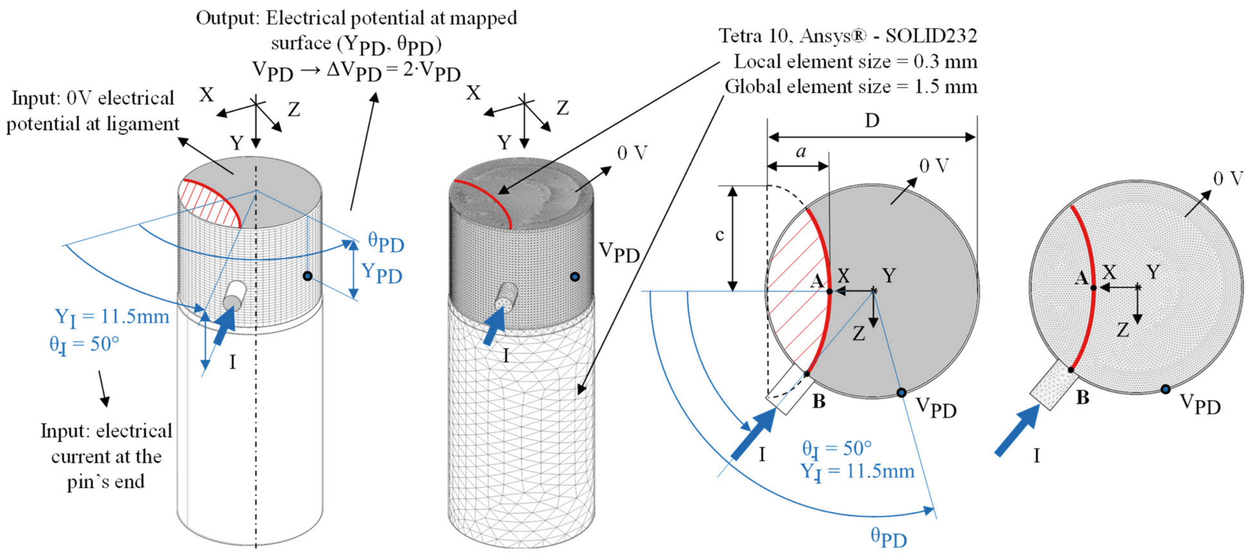

Fig. 8. 3D electrical FE analyses for calibrating the potential drop method: local current input ($Y_I = 11.5$ mm, $\theta_I = 50°$).

To analyse the effect of the potential probes location in all previous current configurations, the outer cylindrical surface of the specimen was mapped to obtain the electrical potential drop at different positions all over it. More in detail, the axial coordinate of the potential probes was varied between 0.5 mm and 18 mm stepped by 0.5 mm and the angular coordinate between -180° and +180° stepped by 5°.

Moreover, to reduce the computational effort, all geometries were modelled by considering the XZ anti-symmetry plane on the specimen net-section. Accordingly, a 0-V-electric-potential was imposed to all the nodes lying on the ligament section area. In addition, no electric contact was assumed between the cracked surfaces. All models except the one with current input located at 50° (see Fig. 8) were modelled taking advantage also of the XY symmetry plane.

Afterwards, several FE analyses were performed by varying the crack depth, *a*, from 7 mm to 10 mm with step of 0.1 mm. The semi-elliptical crack shape having an iso-K_I profile was modelled in all FE analyses. Therefore, the crack path was mono-parametric, i.e. fully defined by the crack depth *a*, the aspect ratio *c/a* being reported in Fig. 4. The electrical potential V_{PD} was computed from the FE analyses as a function of the crack depth *a*, the current injection conditions (Y_I, θ_I) and the position of the potential probes (Y_{PD}, θ_{PD}). Finally, the corresponding potential drop ΔV_{PD} was obtained as $\Delta V_{PD} = 2 \cdot V_{PD}$. Table 2 report a summary of all electrical FE analyses performed.

Table 2. Summary of the electrical FE analyses carried out to derive the calibration curves of the potential drop method

a [mm]	D [mm]	*c/a* [-]	I [A]	ρ at 20°C [Ωmm]	Y_I [mm]	θ_I [°]	Y_{PD} [mm]	θ_{PD} [°]
7, 7.1, …, 10	23.6	iso-$K_I$from Fig. 4	50	$20 \cdot 10^{-5}$	∞	0	0.5, 1.0, …, 18	-180, -175, …, +180
					11.5	0		
					4	0		
					11.5	50		

After having solved all FE models, the numerical results were post-processed to calculate the derivative of the potential drop with respect to the crack size (Eq. (2)), i.e. the DCPD sensitivity. To do so, the forward difference method was applied.

Fig. 9 reports the DCPD sensitivity as a function of the potential probes position (Y_{PD}, θ_{PD}) with reference to two different crack size (*a/D* = 0.3 and 0.4) and the four considered current injection configurations.

Dealing with the potential probe location, as shown in Fig. 9, independently from the position of the current probes, the maximum sensitivity occurred when the potential probe was located as close as possible to the crack plane ($Y_{PD} \rightarrow 0$) and at an angle slightly smaller than that corresponding to the crack tip lying on the outer cylindrical surface ($\theta_{PD} \rightarrow \theta_B$ or $\theta_{B'}$). Accordingly, to keep the maximum sensitivity during fatigue crack growth, the potential probe should move to follow the crack tip propagating along the cylindrical surface of the specimen. Similarly, Ritchie et al. (1971), dealing with SEN and CT specimens, observed that locating the potential probes as close as possible to the crack tip would increase the DCPD sensitivity. Results presented in Fig. 9 also showed that, independently from the current injection mode, the sensitivity increased as the distance of the potential probe Y_{PD} decreased, provided that the angular position θ_{PD} is inside the range defined by the crack surface, that is within $\theta_{B'}$ and θ_B. On the other hand, when the potential probe angle θ_{PD} was outside the range defined by the crack surface, i.e. between -180° and $\theta_{B'}$ or between θ_B and +180°, the DCPD sensitivity decreased with decreasing the distance Y_{PD}.

Concerning the current probe location, the DCPD sensitivity increased if the current was injected as close as possible to the crack tip lying on the outer cylindrical surface of the specimen (Fig. 9). This situation could be reached by reducing the distance Y_I of the current probe from the crack plane (see in comparison Fig. 9a, i.e. remote current input, and Figs. 9b and 9c, i.e. local current input) and also by setting the angular position θ_I equal to θ_B or $\theta_{B'}$, (see in comparison Fig. 9b and Fig. 9d), as previously observed for the potential probe. Finally, it should be noted that in the case of Fig. 9d, the distribution of electrical potential was non-symmetric, so that the DCPD sensitivity was maximum at the crack tip side where the current was injected (point B), while it was lower on the opposite side (point B').

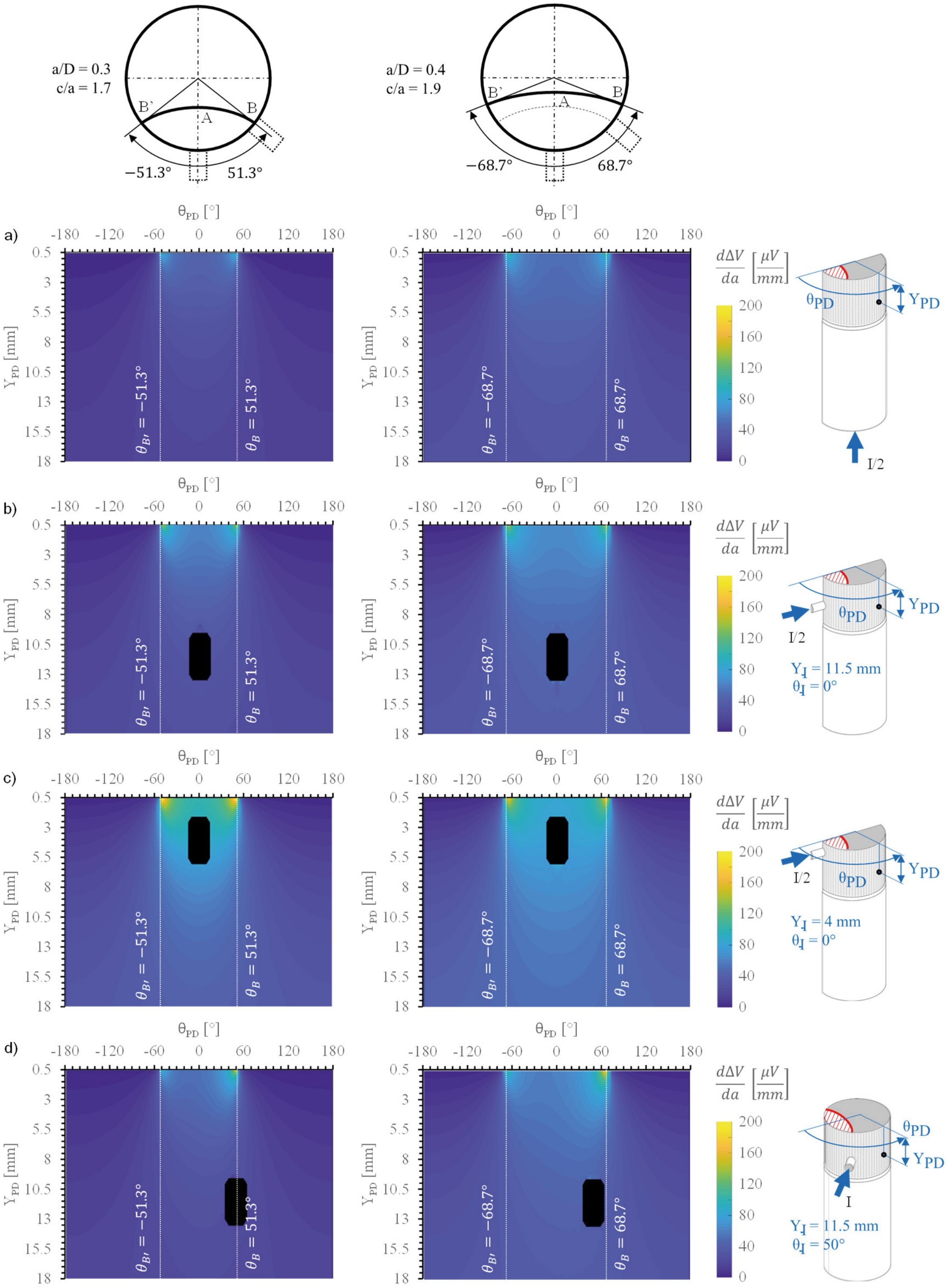

Fig. 9. Sensitivity of the DCPD calibration curves ($d\Delta V_{PD}/da$) evaluated in all FE models as a function of PD probes position and for two different crack sizes: a) remote current input, $Y_I = \infty$, b) local current input, $Y_I = 11.5$ mm and $\theta_I = 0°$, c) local current input, $Y_I = 4$ mm and $\theta_I = 0°$, d) local current input, $Y_I = 11.5$ mm and $\theta_I = 50°$. Black zones in the graphs correspond to the location of the current probe.

Obviously, the in-field applications of the DCPD method during fatigue testing requires that the locations of both current and potential probes are kept fixed. Accordingly, the potential probes should be located in a region which allows to increase the DCPD sensitivity, but also, as suggested by Ritchie and Aronson (1979), in a region which provides a calibration curve almost insensitive to small error in probes positioning. In CT and SEN specimens, such region was identified by Richie et al (1971) as close to the notch mouth as possible, since locating the potential probes close to the crack tip could lead to large measuring errors. Dealing with the considered cylindrical specimen (Fig. 1), a good compromise could be obtained by minimizing the axial distance Y_{PD} and setting $\theta_{PD} = 0°$. In this work, a minimum axial distance Y_{PD} of 0.5 mm was considered, which is compatible with the typical size of the potential probes. By considering $Y_{PD} = 0.5$ mm and $\theta_{PD} = 0°$, the calibration curves relevant to the four considered current injection configurations, are reported in Fig. 10. The potential drop is seen on the order of hundreds to thousands of microvolt, when the crack depth is in the range 7 – 10 mm; therefore it is well measurable by adopting a proper experimental DCPD device (Fig. 10). For comparison, the calibration curves relevant to a potential probe located close to the crack tip of the pre-crack (*a/D* = 0.3, see Fig. 1), i.e. at $Y_{PD} = 0.5$ mm and $\theta_{PD} = 50°$, is reported in Fig. 11. Once again, the potential drop was on the order of hundreds of microvolt and it increased by injecting the current as close as possible to the crack tip where the potential probe was located. Noteworthily, a local current input very close to the crack plane, such as case C in Fig. 10 and 11, although it increases sensitivity, on the other hand it might become very critical. In fact, the potential drop measurement would become strongly affected by the local current density field which is difficult to simulate owing to unpredictable, though small, variations of the contact resistance or uncontrolled positioning errors of the current probes in their seat.

At last, by comparing Figs. 10 and 11, it can be observed that locating the potential probe at $\theta_{PD} = 50°$ provides an higher sensitivity as compared to that of the potential probe at $\theta_{PD} = 0°$, indeed at $\theta_{PD} = 50°$ the sensitivity was on the order of 60-210 μV/mm, while at $\theta_{PD} = 0°$ was in the range 40-80 μV/mm.

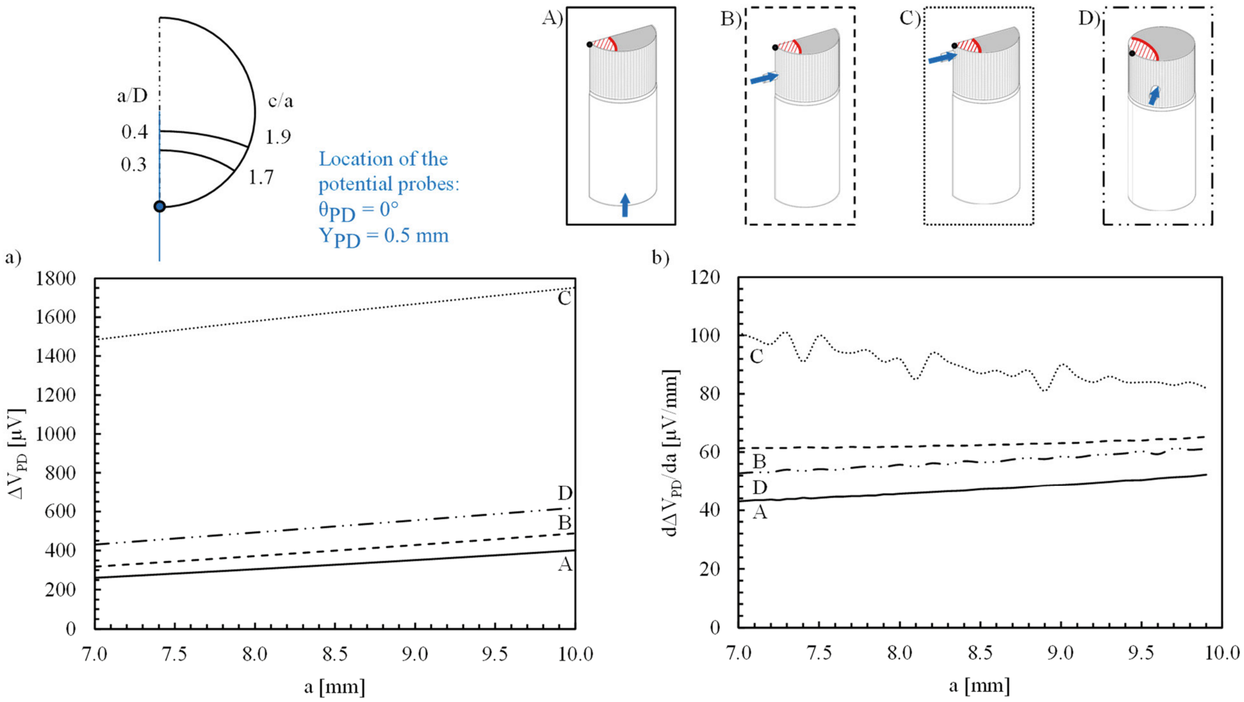

Fig. 10. Comparison between calibration curves obtained from different current probes locations and potential probes located at $Y_{PD} = 0.5$ mm and $\theta_{PD} = 0°$: a) calibration curves; b) sensitivity curves, i.e. derivative of the calibration curves.

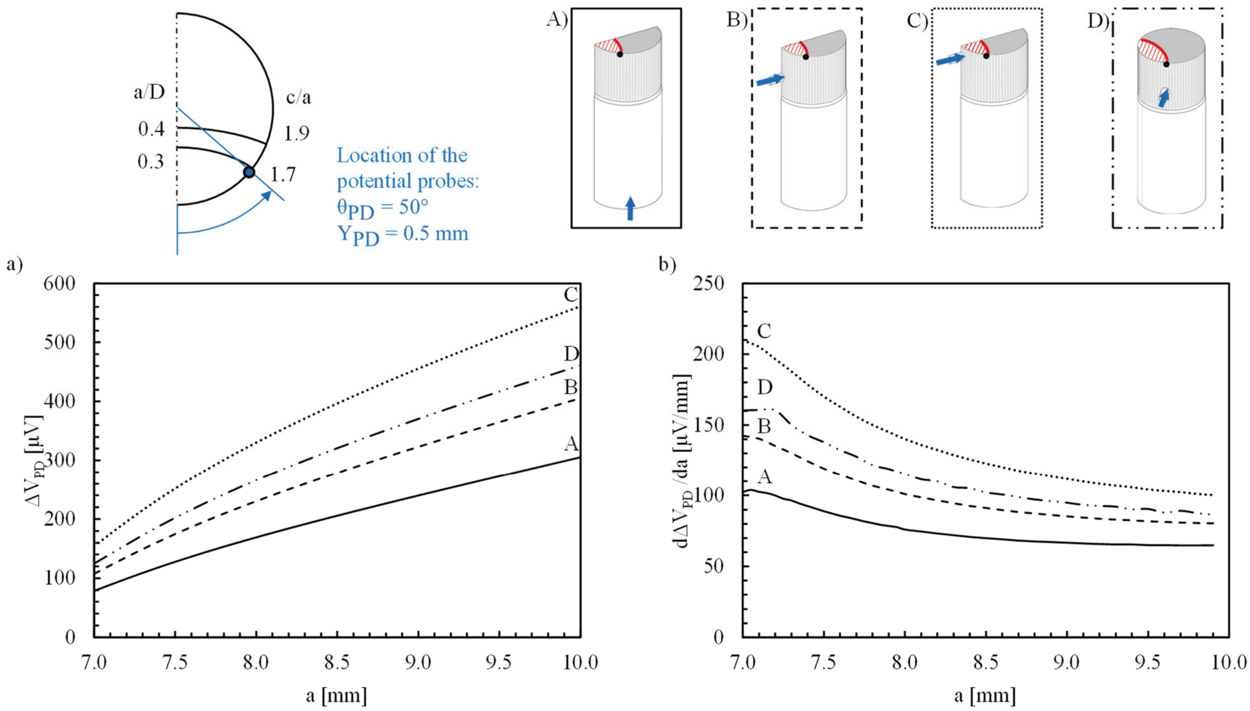

Fig. 11. Comparison between calibration curves obtained from different current probes locations and potential probes located at Y_{PD} = 0.5 mm and θ_{PD} = 50°: a) calibration curves; b) sensitivity curves, i.e. derivative of the calibration curves.

2.3. Resistivity: temperature compensation

The material electrical resistivity could change due to temperature variation of the environment, caused by plastic strain energy dissipation or heat dissipation from the fatigue testing machine. A normalization of the potential drop signal is required to compensate temperature effects. This normalization can be achieved by using the dual channel DPCD technique. Accordingly, the potential drop active channel ΔV_{PD}, measured across the crack as seen in *section 2.2*, is compared to a reference channel ΔV_T, measured on the same specimen. As reported by Doremus et al. (2015), this technique can be adopted provided that the temperature is uniform within the specimen. Two configurations are available: (i) a four-probe dual channel technique (Fig. 12b) as suggested by (Van Minnebruggen et al., 2017), (ii) a three-probe dual channel system (Fig. 12c), in which the reference channel is measured between one probe of the active potential channel and a third probe located on the specimen.

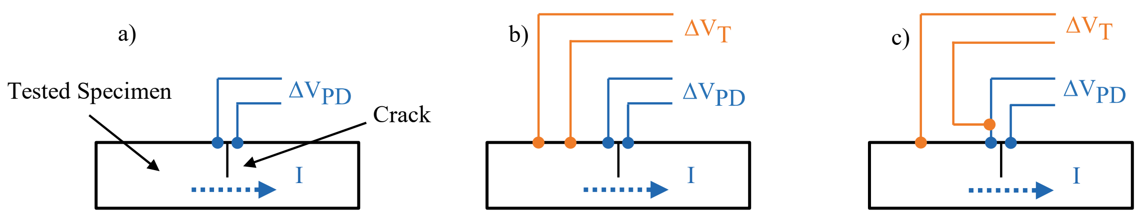

Fig. 12. Different DCPD configuration: a) single channel DCPD setup without in-situ temperature compensation; b) four-probe dual channel DCPD setup and c) three-probe dual channel configuration with in-situ temperature compensation.

From a theoretically point of view, the location of the third probe for temperature compensation can be anywhere on the specimen. For simplicity, in this work the third probe was aligned with the potential probes, i.e. at the same angular position ($\theta_T = \theta_{PD}$), and its axial location Y_T was chosen to be equal to 5 mm. By doing so, the third pin was far enough from the current probe to avoid possible influences of the local current distribution close to the contact region between the current probe and the specimen surface. Moreover, it was far enough also from the active channel probe in order to have a measurable potential drop signal and also a reduced sensitivity to positioning errors.

Taking advantage of previous electric FE analyses, the reference potential drop ΔV_T was calculated as the difference between the electrical potential measured at Y_{PD} = 5 mm ($V_{PD,5mm}$) and the one measured at Y_{PD} = 0.5 mm ($V_{PD,0.5mm}$) so that $\Delta V_T = V_{PD,5mm} - V_{PD,0.5mm}$. The reference potential drop ΔV_T as a function of the crack depth *a* is reported in Fig. 13, where only the case of potential probes located at $\theta_{PD} = \theta_T = 50°$ for all considered positions of the current probes is reported for sake of brevity. On Fig. 13a, calibration curves relevant to the active channel ΔV_{PD} and the reference channel ΔV_T are reported. It is worth noting that both potential drop values are affected by the material electrical resistivity, i.e. by temperature changes, and by the value of the injected current. However, the ratio between these values, $\Delta V_{PD}/\Delta V_T$, provides the normalized calibration curves shown on Fig. 13b, which depended only on the specimen geometry, the crack shape and the current and potential probe locations.

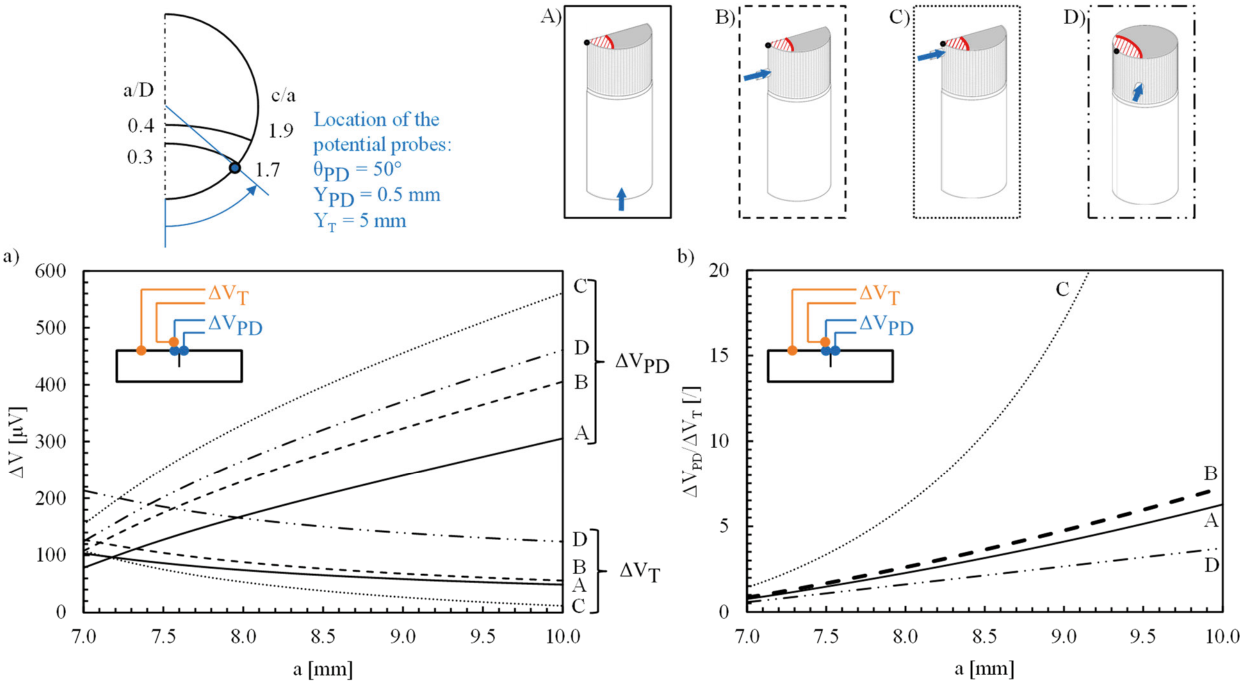

Fig. 13. Normalized calibration curves obtained from different current injection configurations and potential drop probes located at Y_{PD} = 0.5 mm and θ_{PD} = 50°: a) calibration curves relative to the active channel (ΔV_{PD}) and the reference channel (ΔV_T); b) normalized calibration curves ($\Delta V_{PD}/\Delta V_T$).

Conclusions

A numerical investigation on the calibration of the DCPD method for crack growth monitoring in fatigue tests of round bars, made of carbon steel and weakened by a single-edge semi-elliptical pre-crack was performed.

The crack shape was supposed semi-elliptical and the corresponding crack pattern was assumed to guarantee an iso-K_I crack tip profile. Accordingly, the iso-K_I crack shape was derived by means of 3D structural FE analyses performed varying the normalized crack depth *a/D* and the aspect ratio *c/a*. The mode I SIF values were computed by applying the PSM to FE models where the effect of machine grip was modelled as either simply supported or absent. It was shown that the crack pattern is almost insensitive to the applied boundary conditions.

The calibration curves for the application of the DCPD method to the considered specimen geometry were calculated by means of 3D electrical FE analyses by assuming the iso-K_I crack shape determined by means of the structural FE analyses. The performed electrical FE models analysed the effects of the potential and the current probe location on the calibration curve. In agreement with the published literature relevant to SEN and CT specimens, it was shown that the maximum sensitivity is achieved not only by injecting the current, but also by measuring the potential drop as close to crack tip as possible.

Finally, the effect of temperature on the calibration curves was discussed; as a result, a three-probe dual channel normalization technique was proposed to compensate the effects of temperature variations during the fatigue test.

References

Aronson, G.H., Ritchie, R.O., 1979. Optimization of the Electrical Potential Technique for Crack Growth Monitoring in Compact Test Pieces Using Finite Element Analysis. Journal of testing and evaluation 7, 208-215.

ASTM E 647-15, 2015. Standard test method for Measurement of Fatigue Crack Growth Rates. American Society for Testing and Materials (ASTM)

Campagnolo, A., Meneghetti, G., Berto, F., Tanaka, K., 2018. Calibration of the potential drop method by means of electric FE analyses and experimental validation for a range of crack shapes. Fatigue Fract. Eng. Mater. Struct. 41, 2272–2287. https://doi.org/10.1111/ffe.12856.

Campagnolo, A., Roveda, I., Meneghetti, G., 2019. The Peak Stress Method combined with 3D finite element models to assess the fatigue strength of complex welded structures. Procedia Struct. Integr. 19, 617–626. https://doi.org/10.1016/j.prostr.2019.12.067.

Doremus, L., Nadot, Y., Henaff, G., Mary, C., Pierret, S., 2015. Calibration of the potential drop method for monitoring small crack growth from surface anomalies - Crack front marking technique and finite element simulations. Int. J. Fatigue. 70, 178–185. https://doi.org/10.1016/j.ijfatigue.2014.09.003.

Frost, N. E., Pook, L.P., Denton, K., 1971. A fracture mechanics analysis of fatigue crack growth data for various materials. Eng. Fract. Mech. 3, 109–126. https://doi.org/10.1016/0013-7944(71)90003-8.

Meneghetti, G., Lazzarin, P., 2007. Significance of the elastic peak stress evaluated by FE analyses at the point of singularity of sharp V-notched components. Fatigue Fract. Eng. Mater. Struct. 30, 95–106. https://doi.org/10.1111/j.1460-2695.2006.01084.x.

Meneghetti, G., Campagnolo, A., Avalle, M., Castagnetti, D., Colussi, M., Corigliano, P., De Agostinis, M., Dragoni, E., Fontanari, V., Frendo, F., Goglio, L., Marannano, G., Marulo, G., Moroni, F., Pantano, A., Rebora, A., Scattina, A., Spaggiari, A., Zuccarello, B., 2018. Rapid evaluation of notch stress intensity factors using the peak stress method: Comparison of commercial finite element codes for a range of mesh patterns. Fatigue Fract. Eng. Mater. Struct. 41, 1044–1063. https://doi.org/10.1111/ffe.12751.

Ritchie, R.O., Garrett, G.G., Knott, J.P., 1971. Crack-growth monitoring: Optimisation of the electrical potential technique using an analogue method. Int. J. Fract. Mech. 7, 462–467. https://doi.org/10.1007/BF00189118.

Ritchie, R.O., Bathe, K.J., 1979. On the calibration of the electrical potential technique for monitoring crack growth using finite element methods. Int. Journ. Of Fracture 15, 47-55.

Saka, M., Abé, H., Oouchi, A., 1996. NDE of a crack by using closely coupled probes for DCPD technique. J. Press. Vessel Technol. Trans. ASME. 118, 198–202. https://doi.org/10.1115/1.2842181.

Tanaka, K., Akiniwa, Y., 1988. Resistance-curve method for predicting propagation threshold of short fatigue cracks at notches. Eng. Fract. Mech. 30, 863–876. https://doi.org/10.1016/0013-7944(88)90146-4.

Van Minnebruggen, K., Hertelé, S., Verstraete, M.A., De Waele, W., 2017. Crack growth characterization in single-edge notched tension testing by means of direct current potential drop measurement. Int. J. Press. Vessel. Pip. 156, 68–78. https://doi.org/10.1016/j.ijpvp.2017.06.009.

Zerbst, U., Vormwald, M., Pippan, R., Gänser, H.P., Sarrazin-Baudoux, C., Madia, M., 2016. About the fatigue crack propagation threshold of metals as a design criterion – A review. Eng. Fract. Mech. 153, 190–243. https://doi.org/10.1016/j.engfracmech.2015.12.002.